CHAPTER 5

Spin-phonon coupling and giant dielectric constant in $Bi_{0.5}La_{0.5}Fe_{0.4}Al_{0.1}Mn_{0.5}O_3$

5.1 INTRODUCTION

The investigation of phase transitions in disordered magnetic systems is a long-standing subject in solid-state and materials research. Nowadays, spin frustration in magnetic systems has attracted a great deal of attention, both for their theoretical underpinnings and potential applications. The presence of these effects leads to the random freezing of the spin degrees of freedom at the microscopic scale without the usual long-range order[1]. The random freezing of the spin eventually drives the system to go through a spin-glass (SG) transition, which is a well-known phenomenon observed in magnetic systems. Several multiferroic systems have been discovered in which an SG phase was observed. Multiferroic systems such as pure $BiFeO_3$ [220] and disordered $BiFeO_3$[221] and some site-disordered compounds like $PbFe_{1/2}Nb_{1/2}O_3$[222] have been reported to undergo a transition from long-range ordered AFM phase to SG phase at low temperatures with the coexistence of long-range ordered and SG phases in the ground state[41].

Among the above-mentioned materials, bismuth ferrite ($BiFeO_3$) is one of the most researched multiferroic (MF) materials due to its fundamental multiple-order parameter coupling phenomena and numerous applications in magnetoelectric devices with electrically controlled magnetism[6]. Moreover, $BiFeO_3$ (BFO) is the only MF ingredient with a single phase that comprises ferroelectricity and antiferromagnetic (AFM) ordering at room temperature (RT). The magnetization in BFO arises usually due to Fe^{3+}–O^{2-}–Fe^{3+} super-exchange interaction whereas ferroelectricity originates owing to Bi $6s^2$ lone pair electrons. Such materials having both electric and magnetic orders have been receiving a lot of attention in the research world because of their potential for practical applications in next-generation spintronic devices[224]. The two major components of these electronic devices consisted of permanent magnetic data storage systems (hard disc and memory card)

and semiconductor integrated circuits (such as microprocessors and random-access memory). Electronic parts including diodes, resistors, capacitors, and transistors are placed together in a single chip to create semiconductor integrated circuits[1].

In this work, we examine the structural, magnetic, and dielectric characteristics of $Bi_{0.5}La_{0.5}Fe_{0.4}Al_{0.1}Mn_{0.5}O_3$ synthesized using a solid-state technique. At low temperatures, the observed zero field-cooled (ZFC) and field-cooled (FC) magnetization curves show spin-glass behavior. The observation of a cusp at the freezing point, which drops with higher frequencies in the ac susceptibility data, is another confirmation of the SG behavior in BFO. The magnetic results further show that there is strong ferromagnetism in BFO at 5 K. Temperature-dependent Raman measurement shows the spin-phonon (lattice) coupling (SPC) behavior which is an interesting feature of condensed matter physics that arises from the modulation in the phonon modes near magnetic ordering.

5.2 EXPERIMENTAL DETAILS

The polycrystalline powder of $Bi_{0.5}La_{0.5}Fe_{0.4}Al_{0.1}Mn_{0.5}O_3$ was prepared by the traditional solid-state reaction process. In this procedure, highly pure (> 99.9%) Bi_2O_3, Fe_2O_3, La_2O_3, Mn_2O_3, and Al_2O_3 oxides were taken in a stoichiometric ratio and ground for around two hours using a mortar-pestle. This mixture was heated to 850 °C for 24 hours in a programmed furnace. After being re-ground, pelletized, and sintered at 950 °C for 12 hours, the material was cooled to room temperature while undergoing all heat treatments under air pressure. Rigaku Miniflex II X-ray diffractometer was used to perform X-ray diffraction (XRD) measurements at 300 K. We have refined XRD data by using the Full Prof Suite technique. Magnetization measurements were performed using a magnetic property measurement system (Quantum design MPMS® 3) based on a superconducting quantum interference device (SQUID). Dielectric measurement was performed with a very sensitive Keysight E4980A Precision LCR meter equipped with a He-cooled CCR (closed-

cycle refrigerator). Temperature-dependent (100-300K) Raman spectroscopic studies were accomplished (Model: In Via, Make-Renishaw, UK) to explore the dynamics of phonons and lattice vibration in the backscattering configuration and equipped with Peltier cold charge-coupled device (CCD) as a detector. The solid-state laser with 532 nm wavelength was used as an excitation source to record the Raman data within the range 50-1000 cm^{-1}. For data collection, the sample was exposed to laser excitation using a grating of 2400 gr/mm and a 50×X focusing objective. X-ray photoelectron spectroscopy (XPS) is used with a non-monochromatic Mg K (1253.6 eV) excitation source to evaluate the valence state of the ions in the prepared samples. The monochromatic X-ray source Al-Kα line with photon energy 1486.70 eV and a hemispherical electron energy analyzer (EA 125) were both used to collect the XPS data via an Omicron multi-probe surface research system. A value of 2.810^{-11} Torr was maintained as the average base pressure.

5.3 RESULTS AND DISCUSSIONS

5.3.1 X-RAY DIFFRACTION STUDY:

Figure 5.1 depicts the XRD pattern along with its Rietveld refinement. To extract information about the crystal structure of the recorded XRD pattern, we employed Fullprof-suite software for the Rietveld refinement.

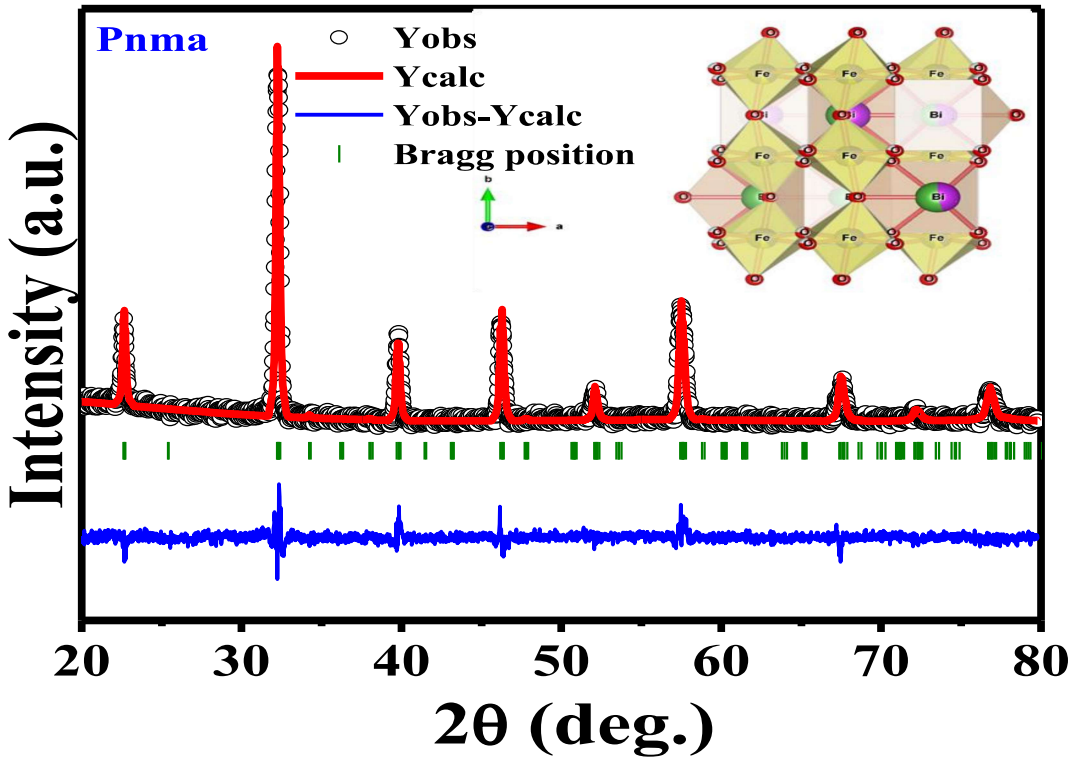

Figure 5.1: *Rietveld refinement of the X-ray diffraction data of $Bi_{0.5}La_{0.5}Fe_{0.4}Al_{0.1}Mn_{0.5}O_3$ system at room temperature with inset showing the 3D structure.*

The solid solution of the Al-doped BLFAMO remained in its original orthorhombic (i.e., $Bi_{0.5}La_{0.5}Fe_{0.5}Mn_{0.5}O_3$) crystal structure with space group Pnma, proving that the 10% doping of Al on the Fe site did not change the crystal structure. A 3D structure of the BLFAMO is depicted in the inset of Figure 5.1 generated by a VESTA image of the atom distribution throughout its site. More bending in the Fe –O –Fe bond has been observed from the VESTA image.

5.3.2 X-RAY PHOTOELECTRON SPECTROSCOPY STUDY:

We performed the XPS measurement to investigate the electronic states of BLFAMO around the Fermi level at 300 K. The survey spectrum of the BLFAMO system is depicted in Figure 5.2(a), and the specifications of each peak have been allocated following the database of the National Institute of Standards and Technology (NIST). It confirmed the presence of Bi, La, Fe, Al, Mn, and O at the surface of BLFAMO. The spectrum did not

show the existence of any other elements except C, indicating the sample purity. To eliminate the charging effect, all XPS data were examined after adjusting the observed binding energies of the elements using the reference line of C 1s at 284.68 eV[96,225]. In the inset of Figure 5.2(a), we have fitted the spin-orbit splitting peaks of Bi $4f_{5/2}$ and Bi $4f_{3/2}$ which are located at the binding energies (B.E.) 164.15 eV and 158.82 eV, respectively. The doublet separation (ΔE) of 5.33 eV is suggesting a +3-oxidation state of Bi in BLFAMO without any traces of metallic Bi in the matrix as shown[198]. The core level Fe 2p XPS spectra are displayed in Figure 5.2 (b). It has two prominent peaks at B.E. 710.40 eV ($2p_{3/2}$) and 723.90 eV($2p_{1/2}$), respectively, with ΔE of 13.5 eV. Fe $2p_{3/2}$ peak has two components located at ~710.10 eV and ~711.78 eV corresponding to Fe^{2+} and Fe^{3+} respectively[200]. Similarly, the fitting of the Fe $2p_{1/2}$ peak is also showing two components which are located at ~723.70 eV and ~725.28 eV respectively. In The Fe2p region, XPS peak fitting confirms that Fe exists in two mixed valence states, i.e., Fe^{2+} and Fe^{3+}. The satellite peak difference is more than 8 eV above the main peak (Fe $2p_{3/2}$) which corresponds to Fe^{3+}cations suggesting the dominant presence of trivalent Fe ions in our system[226,227].

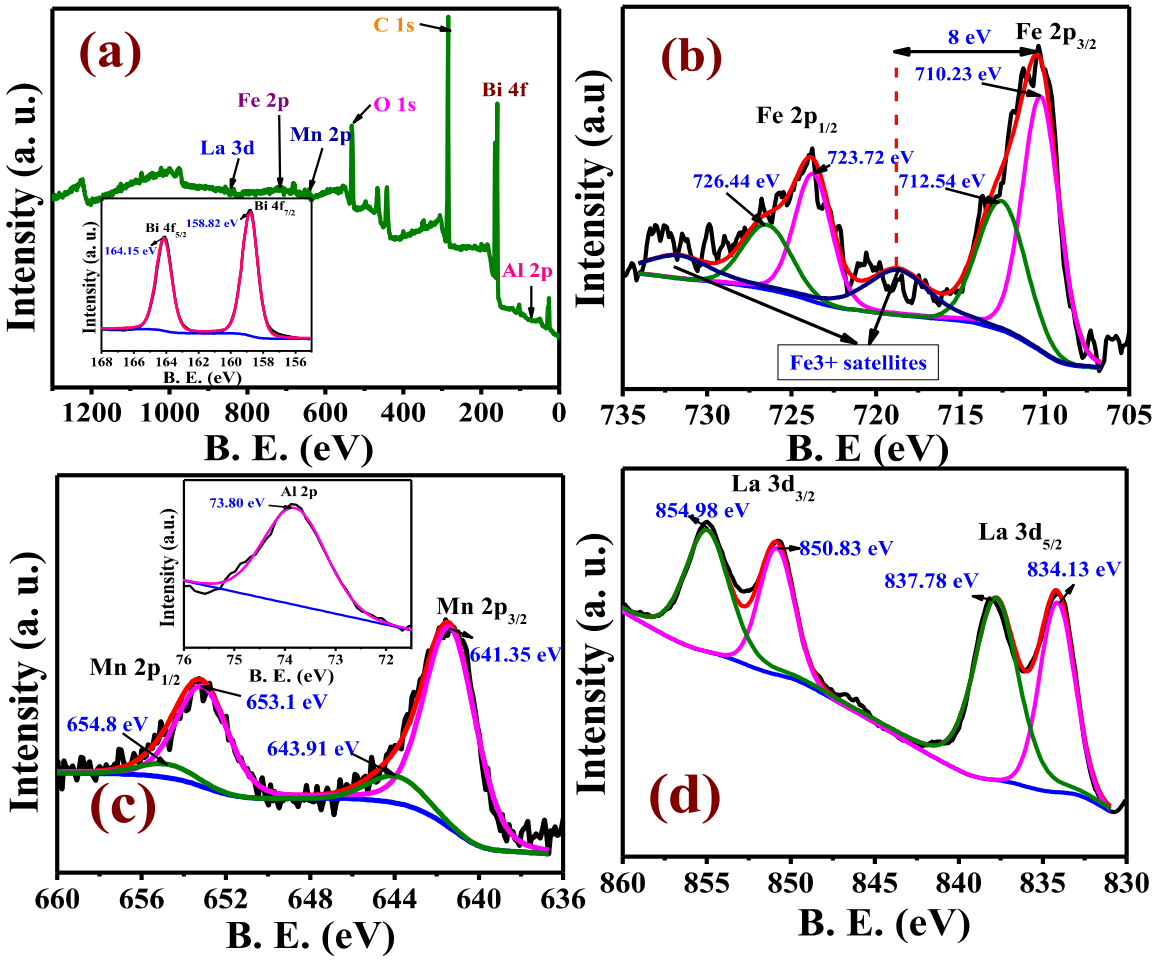

Figure 5.2: *The core level x-ray photoelectron spectroscopy (XPS) of* $Bi_{0.5}La_{0.5}Fe_{0.4}Al_{0.1}Mn_{0.5}O_3$ *system (a) survey scan and in inset Bi 4f, (b) Fe 2p, (c) Mn 2p in inset Al 2p and (d) La 3drespectively.*

The core-level Mn 2p XPS spectrum of the composition is displayed in Fig. 5.2 (c). The main peak of $Mn2p_{1/2}$ (i.e., at B.E. 641.48 eV) and $Mn2p_{3/2}$ (i.e., at B.E. 653.28 eV) with ΔE is determined to be approximately 11.8 eV. The $Mn2p_{3/2}$ deconvolutes into two peaks at B.E. 641.35 eV (Mn^{3+}) and 643.91 eV (Mn^{4+}), whereas $Mn2p_{1/2}$ also deconvolutes into two peaks at B.E. 653.1 eV (Mn^{3+}) and 654.8 eV (Mn^{4+})[228,229]. The Mn2p region XPS peak fitting confirms that Mn also exists in two mixed valence states. In our system, XPS spectra demonstrate that Mn exists in mixed valence states (Mn^{3+} and Mn^{4+}). The inset of Fig. 5.2 (c) shows the XPS spectra of Al at B.E. 73.80 eV which confirms that there is a substitution of Al at the Fe site. La 3d core-level spectra display extremely intricate multi-component

structures. It is understood that a spin-orbit interaction caused the La 3d core level to divide into the $3d_{5/2}$ and $3d_{3/2}$ components. In response to the charge transfer from the bound oxygen to the empty La 4f state, the La $3d_{5/2}$ and La $3d_{3/2}$ peaks are bifurcated further. La 3d XPS spectra are split into 834.13 eV, 837.78 eV, 850.83 eV, and 854.98 eV respectively in which the first two peaks correspond to $La3d_{3/2}$ and last two peaks correspond to $La3d_{5/2}$ as shown in fig. 5.2 (d), suggesting that La exists in a 3+ valence state[18]. The random distribution of Mn, Fe, and Al ions produces numerous competing interactions because of the mixed oxidation states, which is an important factor in the formation of FM clusters in our system (discussed in the magnetic study).

5.3.3 MAGNETIC STUDY:

Figure 5.3 (a) depicts the traditional ZFC and FC magnetization (M) with applied dc field (H) at 500 Oe and 1000 Oe in the temperature range of 2-300 K. From this figure, we observed a sharp rise in moment value below 147 K, which indicates the onset of a long-range magnetic transition. Moreover, a bifurcation between ZFC and FC magnetization has been observed in decreasing the temperature (at the temperature T_p ~ 42 K at 500 Oe and ~32 K at 1000 Oe) in both curves. The bifurcation temperature (T_p) decreases with increasing H, which might be associated with another magnetic transition viz spin freezing. The irreversible temperature which is denoted as T_p is the temperature at which bifurcation occurs and is the onset of thermomagnetic irreversibility [19]. The decrement in T_p towards lower temperatures and the drop in $\Delta\chi'$ is the signature of the frozen spin-glass (SG) transition below T_p[60]. However, it is not a necessary property of a conventional spin-glass, which may alternatively result from the domain structure of a ferromagnetic material or magnetic anisotropy. We have performed the AC susceptibility measurements to shed some light on the origin of this behavior of magnetization of BLFAMO (discussed later)[231].

Further, we identify the accurate transition temperature T_C, from the temperature-dependent (dM/dT) curve which shows the inflection point at 147 K, which is presented in Fig. 5.3 (b).

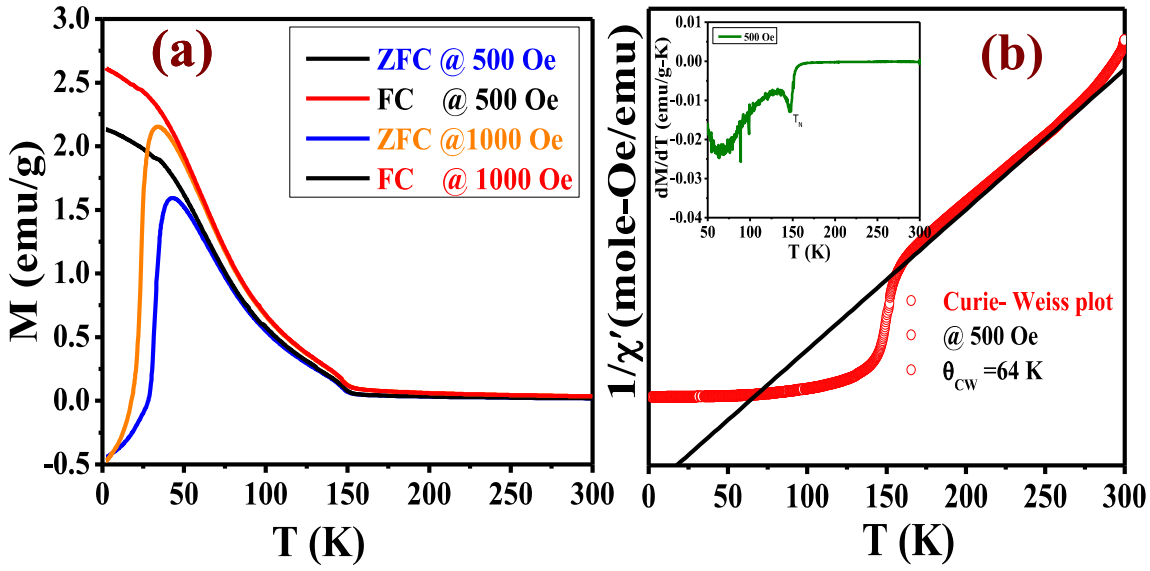

Figure 5.3: *(a) Moment vs. temperature curves measured for zero field cooling and field cooling conditions at 500 Oe and 1000 Oe in the temperature range 2K – 300K. The inset demonstrates temperature-dependent dc susceptibility χ(T) measured under different applied fields for ZFC and FC protocols(b)Showing dM/dT curve, the inset of (b) presents 'Curie–Weiss fit of 1/χ versus T' plot of* $Bi_{0.5}La_{0.5}Fe_{0.4}Al_{0.1}Mn_{0.5}O_3$.

We have also fitted the Curie-Wiess (CW) law as depicted in the inset of Fig. 5.3 (b) on the reciprocal of susceptibility ($1/\chi_{dc}$= H/M) against the temperature curve. The Curie-Wiess law is given by

$$\chi_{dc} = \frac{C}{T-\theta_{CW}} \qquad (1)$$

Here C and θ_{CW} are the Curie constant and CW temperature respectively. From the fitting of equation 1, the θ_{CW} is calculated to be ~ 64 K. The positive value of θ_{CW} signifies dominant ferromagnetic interactions in the system. The huge temperature difference between T_C ~147 K and θ_{CW}~ 64 K suggests that there is spin frustration due to the presence of few AFM phases in addition to the dominant FM interaction. For the glassy systems, the

small value of θ_{CW} represents the sum of all magnetic interactions which depicts the competition between ferromagnetic and antiferromagnetic interactions [63,225,231,232].

For a better understanding of the spin dynamics of the compound, a frequency and temperature-dependent ac magnetic susceptibility (χ'_{ac}) experiment was carried out by applying a fixed ac magnetic field of 3 Oe. The real part of χ'_{ac} as a function of temperature is plotted as shown in Figure 5.4 (a). The χ'_{ac} curve has two distinct peaks at $T_p \sim 42$ K and $T_C \sim 147$ K, indicating two magnetic transitions. It is relevant to mention here that the dc M(T) curves have also shown the two transitions at the same temperatures for the 500 Oe applied field. The inset of Figure 5.4 (a) clearly shows that the peak position, which is observed at the lower temperature side, shifts towards higher temperatures as the frequency increases. Moreover, the peak height also decreases as the applied frequency value increases. It is the characteristic of oxide systems with short-range (i.e., spin-glass type) magnetic interactions[209,233]. The χ'_{ac} peak observed at higher temperatures ($T_C \sim 147$ K) is frequency-independent, suggesting long-range magnetic ordering[14].

To further probe the sensitivity of the applied frequency we estimated the Mydosh parameter, which is strongly influenced by the interactions among the magnetic entities. The Mydosh parameter (S) is considered a universal technique for investigating the glassy state, using the frequency dependency of the ac peaks[234,235]. The Mydosh parameter can be estimated using the expression,

$$S = \frac{\Delta T_p}{T_p \Delta \log_{10} f} \qquad (2)$$

Where $\Delta T_p = (T_p)_{f2} - (T_p)_{f1}$ and $\Delta \log 10(f) = \log 10(f_2) - \log 10(f_1)$. For normal, spin glass (SG) or cluster glass (CG) systems S lies between 0.005 and 0.08, but for the superparamagnetic system, S>0.1. In the present case, the obtained value of S is ~0.05 suggesting the presence of the CG state in the BLFAMO system.

Additionally, in an SG or CG state spin dynamics slows down below the freezing temperature Tp. We can study the essential slowing down of spins at Tp by applying the dynamic scaling law,

$$f = f_0 \left(\frac{T_p - T_G}{T_G}\right)^{z\nu} \quad (3)$$

In this case, f_0 is the excitation frequency corresponding to the typical spin-flip time (τ_0) as $f_0 = 1/\tau_0$; T_G stands for the equivalent freezing temperature in the limit of $H_{DC} \rightarrow 0$ Oe and $f \rightarrow 0$ Hz; the dynamical critical exponent is referred to as '$z\nu$'. The power rule in Eq. (3) can be rewritten as follows to further smooth fitting the data:

$$\log(f) = \log f_0 + z\nu \log\left(\frac{T_p - T_G}{T_G}\right) \quad (4)$$

Figure 5.4 (b) illustrates the "log(f) *vs.* log((T_p-T_G) /T_G)" curve, which shows the linear behavior. The Vogel-Fulcher (VF) law is another phenomenological model that analyses the dynamical scaling of the system by taking into consideration the interaction between relatively larger entities. According to the Vogel-Fulcher law, the freezing temperatures frequency dependency is given by:

$$f = f_0 \exp\left(-\frac{E_A}{k_B(T_p - T_0)}\right) \quad (5)$$

Where E_A is the activation energy, k_B is Boltzmann Constant and T_0 indicates the empirical VF temperature commonly regarded as the degree of connection between the dynamic elements. For fitting purposes, this law can be modified by equation (5) and can be written as

$$\ln f = \ln f_0 - \frac{E_A}{k_B(T_p - T_0)} \quad (6)$$

Table 5.1 Shows bifurcation, spin glass temperature and spin-flip time (τ_0) and activation energy

H(Oe)	T_p(K)	T_G(K)	T_0 (K)	$z\nu$	τ_0 (sec)	E_A(meV)
500	42	40.28	37.80	1.85	10^{-5}	16.62

As shown in Fig. 5.4 (b & c), both the power law and V-F law type critical dynamics give the best fits. From both fitting magnitude of τ_0 is ~ 10^{-5}sec which falls in the typical cluster glass category (10^{-5} -10^{-10} s)[219].

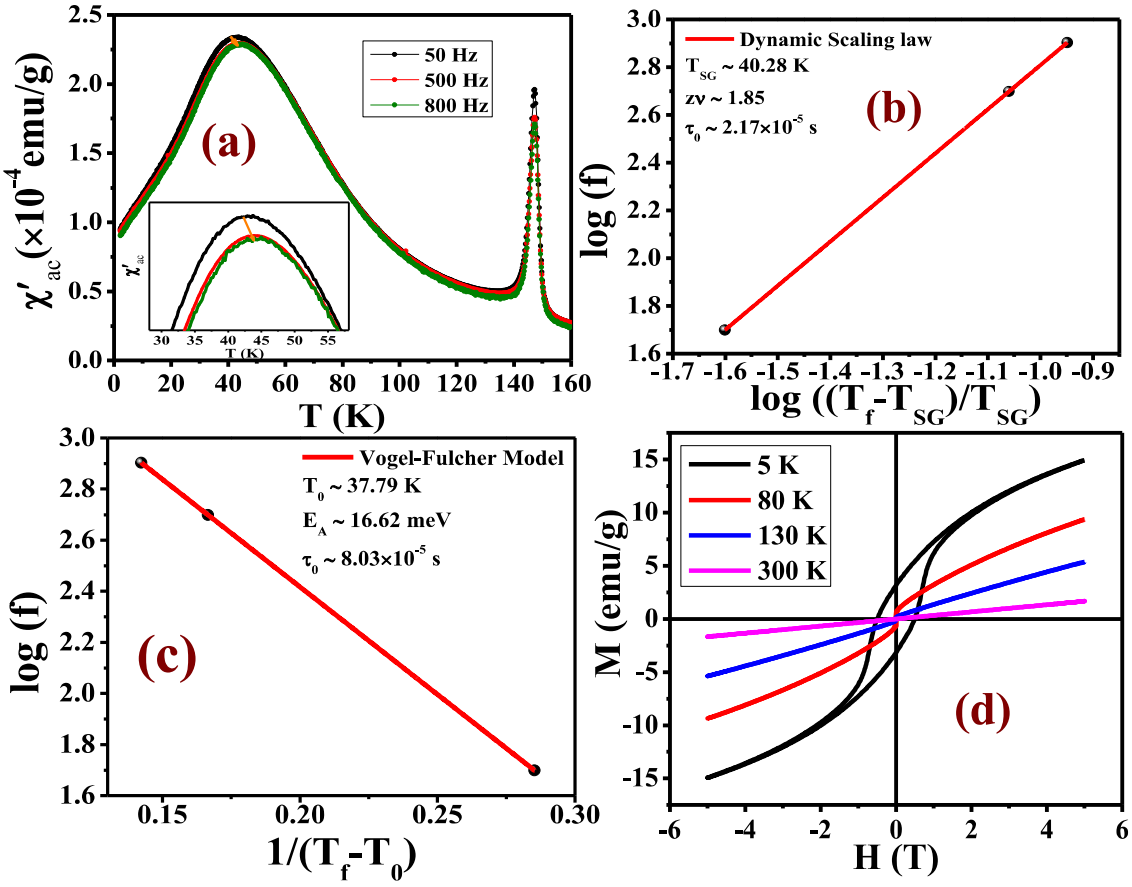

Figure 5.4: *(a) The thermal variation of the real part of ac susceptibility at different frequencies. (b) Demonstrates the dynamic scaling fit to the 'log(f) versus log (Tp-T_G/T_G)' data in the CG region. (c) The plot of log(f) versus 1/(Tp-T_0) fitted with the Vogel–Fulcher law. (d)M (H) curves at 5 K, 80 K, 130 K, and 300 K for $Bi_{0.5}La_{0.5}Fe_{0.4}Al_{0.1}Mn_{0.5}O_3$.*

Moreover, we have acquired the isothermal field-dependent (M-H) loop at various temperatures to better study the magnetic structure of the present system. Figure 5.4 (d) shows the M-H loop recorded at 5 K, 80 K, 130 K (below the magnetic transition temperature), and 300 K. Magnetic moment saturation has not been achieved upto a high applied field of 5T, suggesting the existence of substantial AFM interaction along with FM

interaction in the system except at room temperature (i.e., paramagnetic). The large hysteresis loop is observed at 5 K as compared to the other measured temperature. The canting of Fe^{3+} spins by the Dzyaloshinskii-Moriya interactions, which are frequently seen in orthoferrites might be the origin of the FM hysteretic characteristic[236]. The obtained moment values were enhanced multiple times as compared to the parent $Bi_{0.5}La_{0.5}Fe_{0.5}Mn_{0.5}O_3$ system, which suggests that this material can be used for application purposes.

5.3.4 DIELECTRIC STUDY:

One of the most important features of polycrystalline perovskite materials is their dielectric nature. Studying the dielectric property reveals important details regarding the type of polarization, the relaxation process, the cause of dielectric loss, etc. In this regard, we have measured the dielectric constant (ε') *vs.* temperature shown in Figure 5.5 (a) and the dielectric loss (tanδ) *vs.* temperature curves (shown in the inset of Figure 5.5 (a)) of BLFAMO at a few selected frequencies (1, 5, 10, 50, 100, and 400 kHz). At low temperatures (below 125 K), the ε'-T curve exhibits completely non-dispersive intrinsic polarization and a low value of ε' due to the freezing of dipoles. The value of ε' is 250 at low temperatures (below 125 K), whereas it is of the order of 10^4 at 300 K. Above 125 K, the material exhibits a step-like rising response in ε', and the steps move towards higher temperatures at a higher frequency, exhibiting a thermally triggered polarisation. In general, the rising trend of the dielectric constant for BFO with temperature has been explained by electron-phonon interaction (discussed below). This type of behavior can be explained with the help of Maxwell-Wagner (MW) interfacial polarization as it is typically seen in transition metal oxides[229,237]. At room temperature, the largest dielectric constant value at 1 kHz frequency for parent compound $Bi_{0.5}La_{0.5}Fe_{0.5}Mn_{0.5}O_3$ (BLFMO) [29] was $8x\times10^3$, which has been raised to $1.2\ x\times10^4$ for the BLFAMO system. As we know that the

BFO system has serious leakage current challenges. Doping with rare earth elements has been shown to significantly reduce this leakage problem.

Moreover, we have observed strong relaxation peaks in the dielectric loss spectrum. These peaks move towards higher temperatures at a higher frequency. There is also a weak relaxation peak in the frequency dependence in dielectric spectra showing the signature of relaxor ferroelectricity. The relaxor ferroelectric material also possesses spontaneous polarization similar to normal ferroelectrics but their domains are very small (of the size of the nano-length scale), whereas normal ferroelectric domains are relatively large (of the size on the micro-scale). The overall relaxor-ferroelectricity emerges in the two condensed phases, one of which results due to the formation of polar nano regions (PNRs), and the other one corresponds to the interaction between the PNRs [238]. The PNRs arise due to interaction among dipole moments of the unit cells and form clusters of small polar regions. The size of the clusters of polar regions is of the order of nanoscale, thus they are referred to as polar nano regions. Due to their smaller sizes, polar regions align easily in the direction of applied electric fields. Relaxor ferroelectrics exhibit a high dielectric constant which has been observed in our system and has potential application in the field of energy storage devices[239].

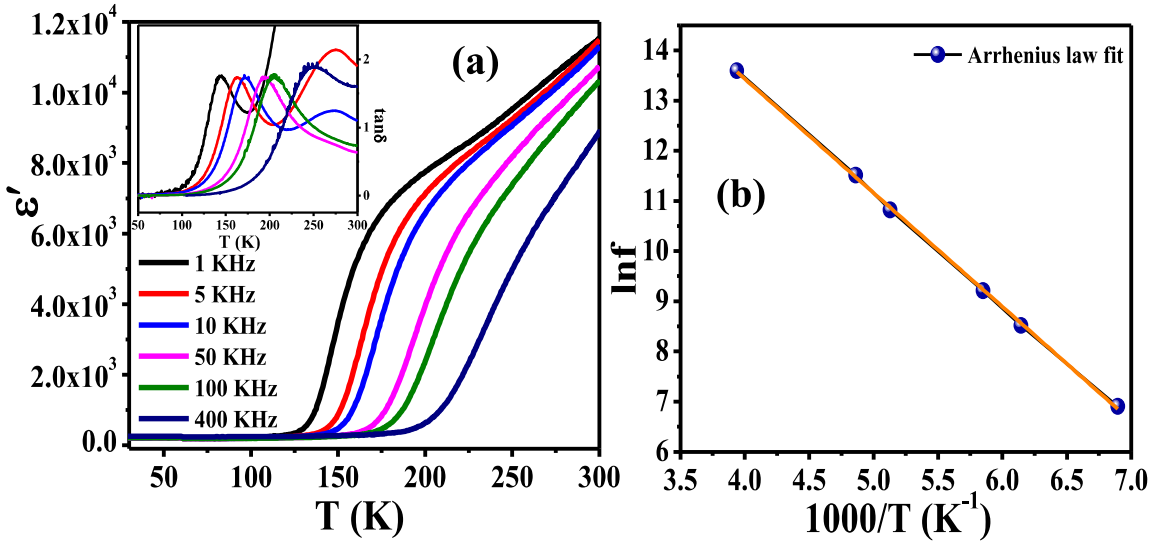

Figure 5.5: *(a) Variation of (a) dielectric constant, and in the inset dielectric loss with the temperature at different frequencies. (b)Arrhenius fits the frequency dependence of the dielectric loss peak for* $Bi_{0.5}La_{0.5}Fe_{0.4}Al_{0.1}Mn_{0.5}O_3$.

Moreover, the Arrhenius equation may be used to study the frequency-dependent nature of the peak position observed in the dielectric loss spectrum. This relation can be written as

$$f = f_0 \exp\left({}^{E_a}/_{K_B T}\right)$$

where E_a is the relaxation activation energy, k_B is the Boltzmann constant, f is the maximum frequency, and f_0 is the peak frequency at a very high temperature. The thermally activated systems are characterized by this rule. The linear relationship between ln(f) and the inverse of temperature is clearly shown in Fig. 5.5 (b), supporting thermally stimulated behavior. The calculated value of activation energy is ~0.19 eV[239,240]. It is important to note that BLFMO did not have such a frequency-dependent dielectric constant or chemical disorder[94].

5.3.5 TEMPERATURE-DEPENDENT RAMAN SPECTROSCOPY: SPIN-PHONON COUPLING

Raman scattering can be utilized as a diagnostic tool for a variation in the local structure that is sensitive to the local disorder, electron-phonon coupling, spin-phonon coupling (SPC), and so on. We have illustrated the experimental Raman spectra for BLFAMO. Figure 5.6 (a) is showing the Raman shift at room temperature (300 K) in the frequency range 200 -1000 cm^{-1}. From this figure, we can see that there are two prominent Raman peaks positioned at frequencies ω_1~ 488 cm^{-1} and ω_2~ 655 cm^{-1} along with many other weak Raman peaks. The peak at ~488 cm^{-1} refers to anti-stretching vibrations, while the band peak at ~ 655 cm^{-1} belongs to stretching vibrations of the transition metal (Fe/Mn) ions octahedra[231]. Moreover, to see the effect of magnetic ordering on phonon modes, we have collected the Raman spectra at different temperatures in the range of 100 K to 300 K. The

inset of Figure 5.6 (a) shows the Raman spectra at different temperatures ranging from 100 K to 300 K for the most intense peak (~ 655 cm^{-1}). However, we did not observe any additional peak with the variation in the temperature, thus indicating that the material's crystal structure remains intact.

Figure 5.6 (b) displays the analysis of the temperature-dependent peak position of the most intense Raman band for a better understanding of the influence of magnetic ordering on phonon mode. Interestingly, we have observed sudden softening in the phonon modes near the magnetic transition temperature, suggesting a clear entanglement between magnetic order and phonon degree of freedom. Such unusual deviation from the anharmonic behavior of the phonon frequency occurs below T_C, suggesting that SPC exists in the system. Furthermore, the associated full width at half maximum (FWHM) of Raman modes (for ~ 655 cm^{-1}) are presented in the inset of Fig. 5.6 (b), respectively. An anomaly has been observed in temperature-dependent FWHM, which confirms that there is an SPC in the system[241].

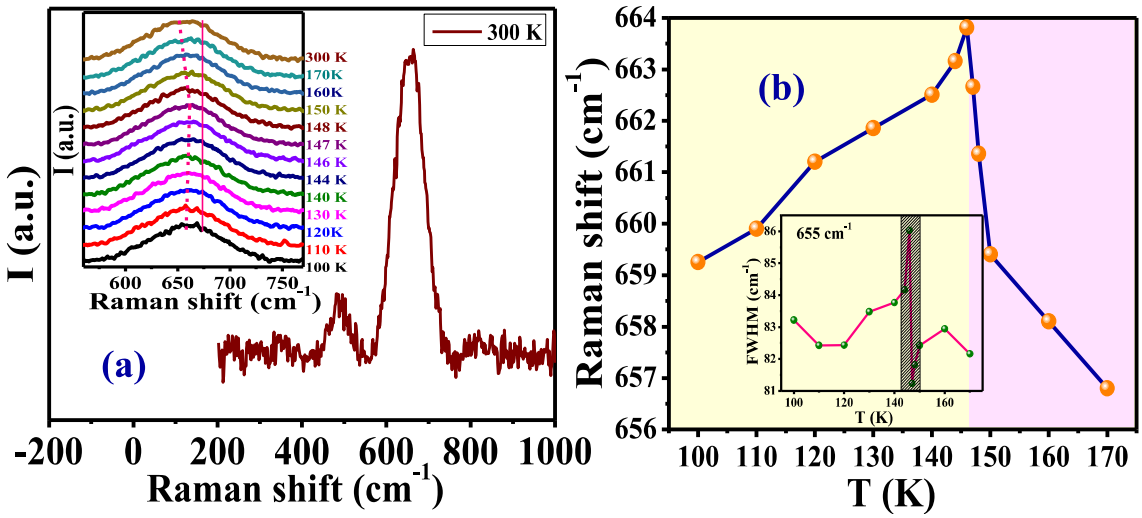

Figure 5.6: *(a) Raman spectra at room temperature and in the inset depicts Raman spectra at different temperatures. (b) Shows the anharmonic behavior to the temperature-dependent Raman shift of stretching mode and in inset presents temperature variation of the FWHM of the stretching mode with an anharmonic behavior for* $Bi_{0.5}La_{0.5}Fe_{0.4}Al_{0.1}Mn_{0.5}O_3$.

5.4 CONCLUSION

The polycrystalline perovskite $Bi_{0.5}La_{0.5}Fe_{0.4}Al_{0.1}Mn_{0.5}O_3$ prepared through the solid-state reaction method adopts a single orthorhombic phase with space group Pnma. The $Bi_{0.5}La_{0.5}Fe_{0.4}Al_{0.1}Mn_{0.5}O_3$ exhibits a second order dominating ferromagnetic ordering below 147 K. Moreover, the dynamic magnetic characteristics of this system using frequency-dependent ac susceptibility measurement show an additional magnetic anomaly (diffused peak) near 40 K along with a sharp peak at 147 K. The analysis of this behavior suggests that the peaks, which reveal a magnetic anomaly near 40 K are linked to a re-entrant glassy dynamic and the peak observed at 147 K is owing to long-range magnetic ordering. The estimated value of the Mydosh parameter was found to be ~0.05 with a relaxation time of $\sim 10^{-5}$ seconds confirming the presence of cluster-glass-like phenomena at low temperatures. The shifting of freezing temperature with the frequency of ac magnetic field is clearly explained by the Vogel-Fulcher and power law. More interestingly, $Bi_{0.5}La_{0.5}Fe_{0.4}Al_{0.1}Mn_{0.5}O_3$ shows a high dielectric constant which is seemingly associated with the presence of relaxor-ferroelectricity. Additionally, $Bi_{0.5}La_{0.5}Fe_{0.4}Al_{0.1}Mn_{0.5}O_3$ material exhibits a spin-phonon coupling, which is seen from the temperature-dependent Raman shift. The presence of the spin glass phenomenon, high dielectric constant, and SPC strongly suggest that the system is a potential candidate for application purposes.